

**A transition state resonance radically reshapes angular
distributions of the $F + H_2 \rightarrow FH(v_f = 3) + H$ reaction in the
62.09 – 101.67 meV energy range**

Dmitri Sokolovski^{a,b,c,*}, Dario De Fazio^d, and Elena Akhmatskaya^{b,e}

^a *Departamento de Química-Física Química-Física,*

Universidad del País Vasco, UPV/EHU, 48940, Leioa, Spain

^b *IKERBASQUE, Basque Foundation for Science, Plaza Euskadi 5, 48009, Bilbao, Spain*

^c *EHU Quantum Center, Universidad del País Vasco, UPV/EHU, 48940, Leioa, Spain*

^d *Istituto di Struttura della Materia-Consiglio Nazionale delle Ricerche, 00016 Roma, Italy and*

^e *Basque Center for Applied Mathematics (BCAM),*

Alameda de Mazarredo 14, 48009, Bilbao, Spain

(Dated: August 30, 2024)

ABSTRACT

Reactive angular distributions of the benchmark $F + H_2(v_i = 0) \rightarrow FH(v_f = 3) + H$ reaction show unusual propensity towards small scattering angles, a subject of a long debate in the literature. We use Regge trajectories to quantify the resonance contributions to state-to-state differential cross sections. Conversion to complex energy poles allows us to attribute the effect almost exclusively to a transition state resonance, long known to exist in the $F + H_2$ system and its isotopic variant $F + HD$. For our detailed analysis of angular scattering we employ the package `DCS_Regge`, recently developed for the purpose [*Comp. Phys. Comm.*, 2022, **277**, 108370.]

Reactive differential cross sections (DCS) are known to be sensitive to the details of reaction mechanism and are, therefore, a source of useful information. A simple picture of a collision between an atom and a diatomic molecule is as follows (see, e.g., [1]). In atom-diatom reaction, transfer of an atom is more likely when the distance between the collision partners is short, i.e., for small angular momenta, or small impact parameters. With the forces acting between the atoms being of predominantly repulsive nature, a rapid encounter

* dgsokol15@gmail.com

between the reactants is likely to favour large reactive scattering angles θ_R . Such a direct mechanism can, therefore, be expected to produce a backward-peaked reactive DCS, rapidly decreasing as θ_R tends to 0.

This is, however, not what one observes for certain transitions of the benchmark reaction $F + H_2 \rightarrow FH + H$ [2], [3], [4]. Contrary to the above expectation, the DCS for rovibrational manifolds $v_i = 0, j_i = 0 \rightarrow v_f = 3, j_f = 0, 1, 2$ exhibit a high forward ($\theta_R = 0$) peak, followed by pronounced oscillations which affect the entire angular range $0^\circ \leq \theta_R \leq 180^\circ$. The question whether resonances can lead to observable effects in the $F + H_2$ reaction has long been debated in the literature [4], with opposing views expressed by the authors of Refs. [5]-[10] and [3], [11]-[15]. Reactive DCS can be expected to bear witness of resonance behaviour [3] and deserve, therefore, a careful examination.

The question is best settled by an analysis, capable of both quantifying an effect and unambiguously linking it to a known resonance possessed. Recently, a study of three $F + H_2 \rightarrow FH + H$ zero-helicity transitions, $\Omega_i = \Omega_f = 0$, at a translational energy of 62.09 meV, related the unusual behaviour of the state-to-state reactive DCS to the presence of a single Regge pole [16]. The purpose of this paper is to confirm this hypothesis and complete the analysis of Ref.[16] by extending it to a broader energy range 62.09 – 101.67 meV. We obtain the relevant Regge trajectories and, by converting Regge poles into poles in the complex energy plane, attribute the effect to just one transition state resonance [12], known to exist for the $F + H_2$ system and its isotopic variant $F + HD$ (see, for example, Refs.[17]-[19]).

I. METHODS

For our analysis we will rely on a methodology somewhat different from those used in [16]. It was recently implemented in the software `DCS_Regge`, now available in the public domain [20]. The method is discussed in detail in [20], and here we only repeat what is necessary for the present narrative. A differential cross section (DCS), $\sigma_{\nu_f \leftarrow \nu_i}$, at an angle θ_R and an energy E is given by an absolute square of the scattering amplitude,

$$\sigma_{\nu_f \leftarrow \nu_i}(\theta_R, E) = |f_{\nu_f \leftarrow \nu_i}(\theta_R, E)|^2, \quad (1)$$

where the composite indexes $\nu_i = (v_i, j_i, \Omega_i)$ and $\nu_f = (v_f, j_f, \Omega_f)$ include the initial and final vibrational (v), rotational (j) and helicity (Ω) quantum numbers of the system. In the zero-helicity case, $\Omega_i = \Omega_f = 0$, the amplitude is given by a simple partial wave sum,

$$f_{\nu_f \leftarrow \nu_i}(\theta_R, E) = (ik_\nu)^{-1} \sum_{J=0}^{\infty} (J+1/2) S_{\nu_f \leftarrow \nu_i}^J(E) P_J(\cos(\pi - \theta_R)), \quad (2)$$

where J is the total angular momentum quantum number, $S_{\nu_f \leftarrow \nu_i}^J$ is a body-fixed scattering matrix element, $k_\nu \equiv k_{v_i, j_i}$ is the initial translational wave vector of the reactants, and $P_J(\bullet)$ is Legendre polynomial (see, e.g., [21]). In practice, the sum is terminated at some $J = J_{max} \gg 1$, and this inequality holds under the semiclassical condition, assumed throughout the rest of the paper.

For a chosen state-to-state transition, the code `DCS.Regge` evaluates two ‘‘unfolded’’ amplitudes (the usual shorthand notation $\lambda \equiv J + 1/2$ is used below),

$$\begin{aligned} \tilde{f}(\varphi, E) &= \int_0^\infty \sqrt{\lambda} S_{\nu_f \leftarrow \nu_i}(\lambda, E) \exp(i\lambda\varphi) d\lambda, \\ \tilde{g}(\varphi, E) &= \int_0^\infty \lambda S_{\nu_f \leftarrow \nu_i}(\lambda, E) \exp(i\lambda\varphi) d\lambda, \end{aligned} \quad (3)$$

both are functions of the newly introduced angular variable φ , which varies between $-\infty$ and ∞ . The function $S_{\nu_f \leftarrow \nu_i}(\lambda, E)$ in (3), such that $S_{\nu_f \leftarrow \nu_i}(J + 1/2, E) = S_{\nu_f \leftarrow \nu_i}^J(E)$, $J = 0, 1, \dots, J_{max}$, is the analytic continuation of the S -matrix element into the complex angular momentum (CAM) plane, achieved by means of Padé approximation (more details are given in [22]). The scattering amplitude (2) for $\pi/J_{max} \lesssim \theta_R \lesssim \pi - \pi/J_{max}$ can now be obtained by ‘‘folding back’’ the amplitudes (3) [20],

$$\begin{aligned} f_{\nu_f \leftarrow \nu_i}(\theta_R, E) &= (ik_\nu)^{-1} [2\pi \sin \theta_R]^{-1/2} \sum_{m=-\infty}^{\infty} \tilde{f}(\varphi_m) \exp(-i\pi/4 - im\pi/2) \\ &\equiv \sum_{m=-\infty}^{\infty} f_{\nu_f \leftarrow \nu_i}^{(m)}(\theta_R, E), \end{aligned} \quad (4)$$

where

$$\varphi_m(\theta_R) \equiv (-1)^{m+1} \theta_R + \pi[m + 1/2 + (-1)^m/2]. \quad (5)$$

For $\theta_R = 0$, and $\theta_R = \pi$ one has

$$\begin{aligned} f_{\nu_f \leftarrow \nu_i}(\theta_R = 0, E) &= -k_\nu^{-1} \sum_{m=-\infty}^{\infty} (-1)^m \tilde{g}((2m+1)\pi) \equiv \sum_{m=-\infty}^{\infty} f_{\nu_f \leftarrow \nu_i}^{(m)}(0, E), \\ f_{\nu_f \leftarrow \nu_i}(\theta_R = \pi, E) &= (ik_\nu)^{-1} \sum_{m=-\infty}^{\infty} (-1)^m \tilde{g}(2m\pi) \equiv \sum_{m=-\infty}^{\infty} f_{\nu_f \leftarrow \nu_i}^{(m)}(\pi, E). \end{aligned} \quad (6)$$

The rationale behind Eqs.(4) becomes clear by considering the classical limit of atom-diatom reaction $A+BC \rightarrow AB+C$. The variable of interest is the winding angle φ , i.e., the angle swept in the course of collision by the projection of the Jacobi vector $\mathbf{R}_{A\leftarrow BC}$, drawn from the centre of mass of the BC pair to the atom A, onto the plane perpendicular to the total angular momentum \mathbf{J} (see Supplementary Material A). One can attempt to achieve a semiclassical description by ascribing a probability amplitude to the reactive trajectories leading to all winding angles $\varphi_m(\theta_R)$, consistent with the scattering angle θ_R [cf. Eq.(5)], and adding up the amplitudes in accordance with the basic rule of quantum mechanics. The correct formula (4) contains, however, additional phase factors $\exp(-i\pi/4 - im\pi/2)$, and fails for both small and large scattering angles. The reason for this is the coalescence of winding angles $\pi - \theta_R + 2m\pi$ and $\pi + \theta_R + 2m\pi$ as $\theta_R \rightarrow 0$, and of $\pi - \theta_R + 2m\pi$, and $\pi + \theta_R + 2(m-1)\pi$ as $\theta_R \rightarrow \pi$. With the two angles no longer distinguishable, Eq.(4) must be replaced by one of the Eqs.(6). (A detailed discussion of Eqs.(6) can be found in [23]).

The analysis proceeds by examining the shapes of the two $\tilde{f}(\varphi, E)$ and $\tilde{g}(\varphi, E)$. For a direct reaction one can expect an $\tilde{f}(\varphi, E)$ essentially limited to the interval $0 \leq \varphi \leq \pi$, negligible for $\varphi \approx 0$, considerable for $\varphi \approx \pi$ and, perhaps, having a small extension into the $\varphi < 0$ region due to purely quantum effects. For a reaction, passing through formation of one or several intermediate rotating complexes, $\tilde{f}(\varphi, E)$ is likely to extend also into the $\varphi \geq \pi$ zone. This extension is expected to take the form of one or several “exponential tails”, which resonance CAM (Regge) poles at J_n , $n = 1, 2, \dots$, in the first quadrant of the CAM plane contribute to the integrals in Eqs.(3) [23],

$$\begin{aligned} \tilde{f}(\varphi \geq \pi) &\approx 2\pi i \sum_{n=1}^{N_{res}} \sqrt{\lambda_n} r_n(E) \exp(i\lambda_n \varphi) \equiv \sum_{n=1}^{N_{res}} \tilde{f}_n^{tail}(\varphi), \\ \tilde{g}(\varphi \geq \pi) &\approx 2\pi i \sum_{n=1}^{N_{res}} \lambda_n r_n(E) \exp(i\lambda_n \varphi) \equiv \sum_{n=1}^{N_{res}} \tilde{g}_n^{tail}(\varphi). \end{aligned} \quad (7)$$

In Eq.(7), $r_n(E) \equiv \lim_{J \rightarrow J_n} (J - J_n) S_{\nu_f \leftarrow \nu_i}(E, J)$ is the residue of the S -matrix element at $J = J_n$, and the sum is over N_{res} “physically significant poles”. The notion is, in this context, self-explanatory. Significant one is a pole whose contribution to $\tilde{f}(\varphi \geq 0)$ and $\tilde{g}(\varphi \geq 0)$ is sufficient to cause observable interference effects in the DCS [cf Eqs.(4)]. Such a pole must lie not too far from the real J -axis (or its tail will be too short), and have a sufficiently large residue (or the tail will be too small). Finally, we note that Eqs.(7) are consistent with a picture of a rotating intermediate triatomic complex which continues to decay into products.

Triatomic's moment of inertia I and $\text{Re}[J_n]$ determine its angular velocity, $\omega \approx \text{Re}[J_n]/I$, while $1/\text{Im}[J_n]$ yields the typical rotation angle [20].

Next we check whether for the chosen transitions the unfolded amplitudes in Eqs.(3) have tails described by Eqs.(6), and ascribe every found tail to a Regge pole, or poles, of the S -matrix element. Importantly, we will relate each CAM pole to its complex energy counterpart, and explain the shape of the DCS in terms of the well known $F + H_2$ resonances [9],[14], something not yet done in [16]. (The reader who wants to know the result now can consult the article's title).

II. RESULTS

As in [16], we use the S -matrix elements of the title reaction, computed by the hyperspherical method of [24] on the Fu-Xu-Zhang (FXZ) potential energy surface (PES) [25].

A. The $(0, 0, 0) \rightarrow (3, 0, 0)$ transition. The DCS (1) shown in Fig.1a, exhibits a high forward scattering peak, whose height varies little across the translational energy range 62.09 – 101.67 meV considered here. There are also regular oscillations observed, at all energies, in the entire angular range $0 \leq \theta_R \leq 180^\circ$. A closer inspection reveals much smaller patterns superimposed on the DCS in the regions 65 – 71 meV and 85 – 92 meV (indicated by arrows in Fig.1a). To explain this behaviour we employ the `DCS.Regge` code of Ref.[20]. Both unfolded amplitudes in Eq.(3), $\tilde{f}(\varphi, E)$ and $\tilde{g}(\varphi, E)$, shown in Fig.1b and c, respectively, are smooth functions of φ and E , and have tails which extend into $\varphi \geq 180^\circ$ region and become negligible at $\varphi \sim 500^\circ$. The oscillations in Fig.1a must, therefore, result from interference between the part of \tilde{f} contained in the region $0 \leq \varphi \leq 180^\circ$, and the tail, which we expect to be produced by capture into a metastable state, or states [cf. Eqs.(4) and (7)]. To check whether this is the case, we plot the Regge poles in Fig.1d. There are four Regge trajectories, labelled by Roman numerals, $n = \text{I, II, III, IV}$. For $E = 62.09$ meV, trajectory II contains the pole at $J = 12.49 + 0.95i$, previously found in [16], and we expect it to be the most significant of the four. Indeed, in Fig.1e the difference $\delta|\tilde{f}(\varphi, E)| \equiv |\tilde{f}(\varphi, E)| - |\tilde{f}_{\text{II}}^{\text{tail}}(\varphi, E)|\chi(\varphi - \pi)$, where $\chi(x) = 1$ for $x \geq 0$ and 0 otherwise, practically vanishes for $\varphi \geq 180^\circ$, which shows that the pole II responsible for almost all of $\tilde{f}(\varphi, E)$ $\varphi \geq 180^\circ$ region. The same is true for the difference $\delta|\tilde{g}(\varphi, E)| \equiv |\tilde{g}(\varphi, E)| - |\tilde{g}_{\text{II}}^{\text{tail}}(\varphi, E)|\chi(\varphi - \pi)$, shown in Fig.1f. Thus, there can be little doubt that the tails of both unfolded amplitudes

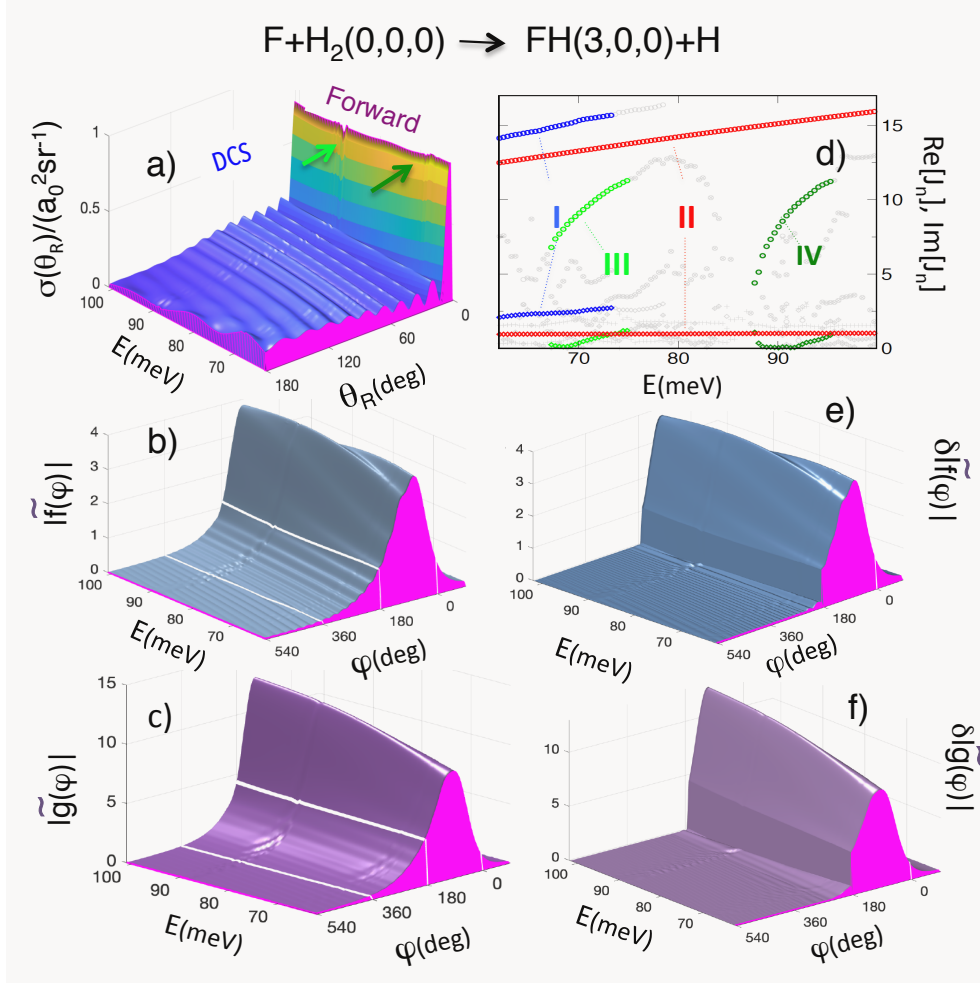


FIG. 1. a) Reactive differential cross section $\sigma_{\nu_i \leftarrow \nu_i}(\theta_R)$ for the $\nu_i = 0, j_i = 0, \Omega_i = 0$ and $\nu_f = 3, j_f = 0, \Omega_f = 0$ vs. θ_R and E . Small patterns which occur in the regions 65 – 70 meV and 85 – 90 meV in the entire angular range are indicated by arrows.

b) The modulus of the unfolded amplitude \tilde{f} vs. the winding angle φ and E .

c) Similar to (b), but for the unfolded amplitude \tilde{g} .

d) Real (circles) and imaginary (diamonds) parts of the four Regge trajectories.

e) The difference between $|\tilde{f}(\varphi)|$ and $|\tilde{f}_{\text{II}}^{\text{tail}}(\varphi)|$ [cf. Eqs.(3) and (7)] subtracted for $\varphi > 180^\circ$.

f) The difference between $|\tilde{g}(\varphi)|$ and $|\tilde{g}_{\text{II}}^{\text{tail}}(\varphi)|$ [cf. Eqs.(3) and (7)] subtracted for $\varphi > 180^\circ$.

and, therefore, the oscillations in the DCS in Fig.1a, are largely caused by the resonance II [cf. Fig.1f].

An inspection of the pole positions in Fig.1d and the corresponding residues in Fig.2 explains why other poles can have only minor effect on $\sigma_{3,0,0 \leftarrow 0,0,0}(\theta_R, E)$. The resonance I (i.e. the

Regge pole I) has the largest residue, but also a large imaginary part. For $\varphi \geq \pi$, its tail, reduced by a factor $\exp\{-\text{Im}[J_I]\varphi\}$, is both short and small. (It needs, however, to be taken into account when calculating the forward scattering cross section at lower energies, as will be shown shortly.) The residues of the poles III and IV are very small, and even though both resonances are long-lived [cf. Fig.1d], they are accountable only for the small patterns indicated by arrows in Fig.1a.

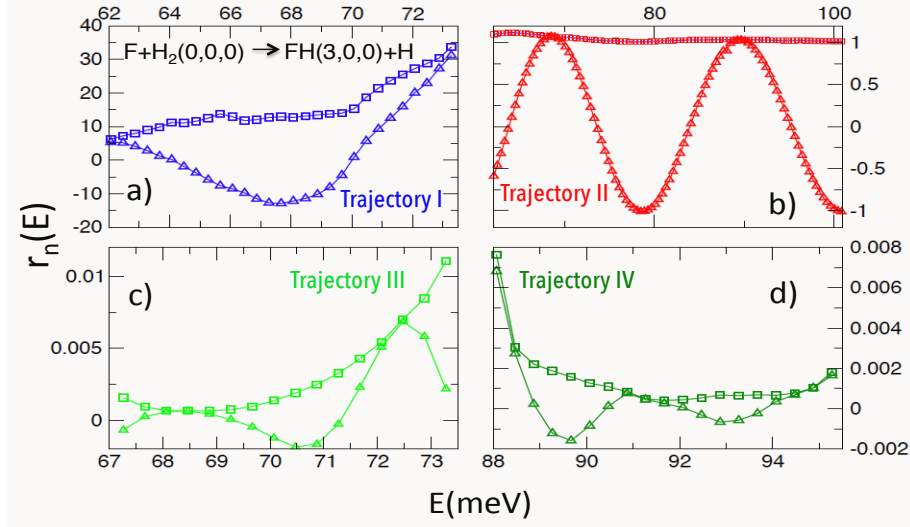


FIG. 2. Moduli (squares) and real parts (triangles) of the residues $r_n(E)$, $n = \text{I, II, III, IV}$, for the four Regge trajectories in Fig.1d.

To quantify the analysis, we consider the energy dependence of the DCS at a chosen scattering angle, first by identifying the important terms in the expansions (4)-(6), using, where possible, approximations (7), and comparing the result with the exact DCS.

A good approximation to the *forward* DCS is obtained by taking into account only the zeroth term in (6), $f_{\nu_f \leftarrow \nu_i}^{(0)}(0, E)$ (orange circles in Fig.3a). One can try to attribute it to the decay of the recently formed resonance II into the forward direction $\theta_R = 0$, $f_{\nu_f \leftarrow \nu_i}(0, E) \approx -k_\nu^{-1} \tilde{g}_{\text{II}}^{\text{tail}}(\pi)$. The result, shown by red circles in Fig.3a, can be improved, by about a fifth (malva circles in Fig.4a), by including also the contribution from the resonance I

$$f_{\nu_f \leftarrow \nu_i}(0, E) \approx -k_\nu^{-1} [\tilde{g}_{\text{I}}^{\text{tail}}(\pi) + \tilde{g}_{\text{II}}^{\text{tail}}(\pi)]. \quad (8)$$

[We are able to follow Regge trajectory I only until it leaves the region where Padé approximation can be trusted at $E \approx 74$ meV [22]. The remaining small discrepancy is attributed to the inaccuracy of the asymptote (7) if the resonance is formed at a large value of J [23]].

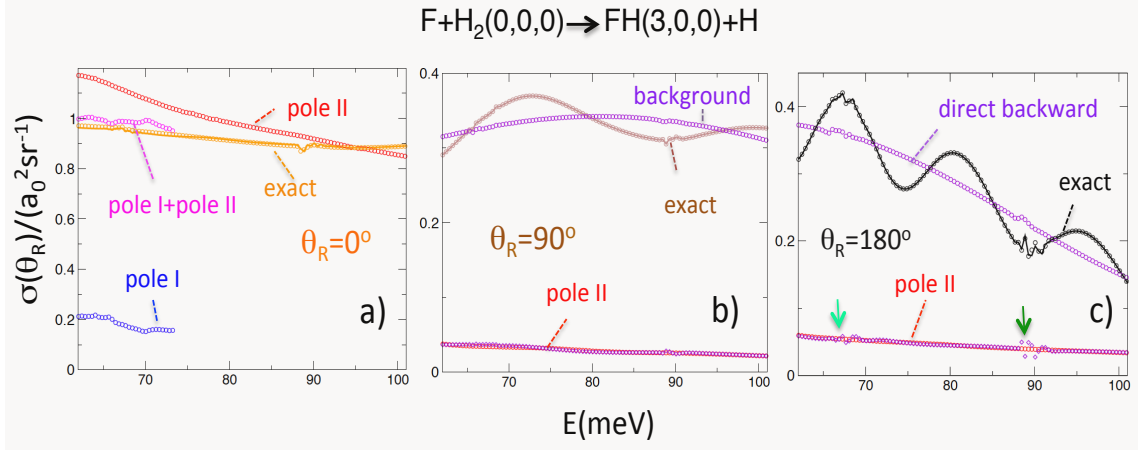


FIG. 3. a) Exact DCS (1) at $\theta_R = 0^\circ$ (solid orange) and $\left|f_{\nu_f \leftarrow \nu_i}^{(0)}(0, E)\right|^2$ (orange circles). Also shown are the resonance contributions $\left|k_\nu^{-2} \tilde{g}_I^{tail}(\pi)\right|^2$ (blue circles), $k_\nu^{-2} \left|\tilde{g}_{II}^{tail}(\pi)\right|^2$, as well as a coherent sum of the two, $k_\nu^{-2} \left|\tilde{g}_I^{tail} + \tilde{g}_{II}^{tail}(\pi)\right|^2$ (malva circles).

b) Exact DCS (1) at $\theta_R = 90^\circ$ (solid brown). Also shown are the background term, $\left|f_{\nu_f \leftarrow \nu_i}^{(-1)}(\pi/2, E) + f_{\nu_f \leftarrow \nu_i}^{(0)}(\pi/2, E)\right|^2$ (violet circles), $\left|f_{\nu_f \leftarrow \nu_i}^{(1)}(\pi/2, E)\right|^2$ (violet diamonds), and their coherent sum $\left|\sum_{m=-1}^1 f_{\nu_f \leftarrow \nu_i}^{(m)}(\pi/2, E)\right|^2$ (brown circles). Contribution of the resonance II, $\left|(2\pi)^{-1/2} k_\nu^{-1} \tilde{f}_{II}^{tail}(3\pi/2) \exp(-i\pi/4)\right|^2$, (red circles) is in good agreement with $\left|f_{\nu_f \leftarrow \nu_i}^{(1)}(\pi/2, E)\right|^2$.

c) Exact DCS (1) at $\theta_R = 180^\circ$ (solid black). Also shown are the direct term $\left|\tilde{f}_{\nu_f \leftarrow \nu_i}^{(0)}(\pi, E)\right|^2$ (violet circles), $\left|\tilde{f}_{\nu_f \leftarrow \nu_i}^{(1)}(\pi, E)\right|^2$ (violet diamonds), and their coherent sum $\left|\sum_{m=0}^1 f_{\nu_f \leftarrow \nu_i}^{(m)}(\pi, E)\right|^2$ (black circles). Contribution of the resonance II, $k^{-2} \left|\tilde{g}_{II}^{tail}(2\pi)\right|^2$ (red circles), is in good agreement with $\left|\tilde{f}_{\nu_f \leftarrow \nu_i}^{(1)}(\pi, E)\right|^2$, with small discrepancies noted where the resonances III and IV need to be taken into account (as indicated by the arrows).

The *sideway* DCS at $\theta_R = 90^\circ$, shown in Fig.3b (solid brown), is, to an excellent accuracy, a result of interference between the “background” term (violet circles), $f_{\nu_f \leftarrow \nu_i}^{(-1)}(-\pi/2, E) + f_{\nu_f \leftarrow \nu_i}^{(0)}(\pi/2, E)$ and $f_{\nu_f \leftarrow \nu_i}^{(1)}(-\pi/2, E)$ (violet diamonds). The latter term is seen to be a result of the decay of the resonance II (red circles) after $\mathbf{R}_{F \leftarrow HH}$ rotates by $3\pi/2$ [cf. Eqs.(6) and (7)],

$$f_{\nu_f \leftarrow \nu_i}(\pi/2, E) \approx f_{\nu_f \leftarrow \nu_i}^{(-1)}(-\pi/2, E) + f_{\nu_f \leftarrow \nu_i}^{(0)}(\pi/2, E) - \frac{1}{\sqrt{2\pi}k_\nu} \tilde{f}_{II}^{tail}(3\pi/2) \exp(-i\pi/4). \quad (9)$$

(Note that DCS_Regge does not distinguish between direct scattering and decay of a resonance for a φ lying between 0 and π . A more sophisticated technique is available [23], but was deemed too cumbersome to be included into the software.)

Finally, the oscillations of the *backward* DCS (black solid) in Fig.3c are clearly the result of interference between a direct recoil following a head-on collision, and the decay of the resonance II after $\mathbf{R}_{F\leftarrow HH}$ completes one full rotation [cf. Eqs.(7)],

$$f_{\nu_f\leftarrow\nu_i}(\pi, E) \approx (ik_\nu)^{-1}[\tilde{g}(0) - \tilde{g}_{II}^{tail}(2\pi)]. \quad (10)$$

B. Assignment of Regge resonances. There are two complimentary ways of relating the same resonance phenomenon to a singularity of a scattering matrix element $S_{\nu_f\leftarrow\nu_i}(\lambda, E)$. Fixing a real value of J allows one to look for poles in complex energy (CE) plane, while fixing a value of E gives rise to CAM Regge poles. The CE poles, whose relation to the PES is usually well understood (see [3], [14],[15]), are not particularly useful for a quantitative analysis of the integral and differential cross sections, given by sums over angular momentum at a fixed value of E . The Regge poles, for their part, are well suited for such an analysis, but can offer little insight into the dynamics on the PES. Fortunately, positions of the poles of one kind can usually be obtained if the positions of poles of the other kind are already known [26], so the benefits of both approaches can be combined.

In the present case, the task is especially easy since the pole positions of the resonances I and II are practically linear functions of E in their respective energy ranges, $J_{I,II} \approx \alpha_{I,II} + \beta_{I,II}E$. Inverting the relation yields the positions of the corresponding CE poles, $E_{I,II}$,

$$E_{I,II}(J) \approx a_{I,II} + b_{I,II}J, \quad (11)$$

with the complex constants given by $a_{I,II} = -\alpha_{I,II}\beta_{I,II}^{-1}$, $b_{I,II} = \beta_{I,II}^{-1}$. Numerical fits, shown in Fig.4, are in good agreement with the exact positions of CE, obtained by Padé reconstruction of the S -matrix element in the complex energy plane. For the $F+H_2$ system, the properties of the CE poles have been extensively studied, e.g., in [14], albeit on a slightly different potential surface. Thus, comparison of Fig.4 and Fig.9 of [14] reveals that the Regge trajectory I and II in Fig.1a correspond to the resonances A and B, a nomenclature first introduced in [9], and subsequently used by other authors (for more detail, see also Supplementary Material B). Both A and B are Feshbach resonances, correlated with bound states with support in different regions of the adiabatic potential curve [cf. Fig.3b of [12]]. Resonance B is a wdW exit channel resonance, while A, trapped in a deeper well lies closer to the system's transition state [11]. It is, therefore, the transition state resonance, with its tails clearly visible in Figs.1b,c, which is responsible for the unusual behaviour of the state-to-state DCS in Fig.1a.

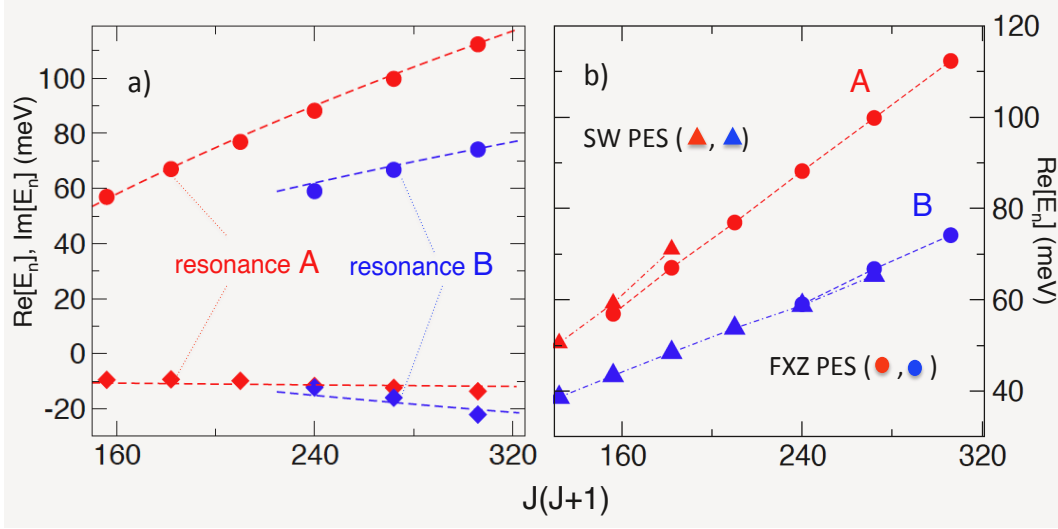


FIG. 4. Real (circles) and imaginary (diamonds) parts of the exact complex energy poles, corresponding to the Regge trajectories I (blue) and II (red) in Fig.1d. Also shown by dashed lines is the approximation (11). The variable $J(J+1)$, rather than J , is used to facilitate comparison with Fig.9 of [14]. b) Comparison between real parts of the CE poles obtained for the FXZ PES (circles, present work), and the corresponding poles for the SW PES (used in Ref.[14], triangles). The SW results are corrected by the energy difference between the two PES.

C. Transitions $(0,0,0) \rightarrow (3,1,0)$ and $(0,0,0) \rightarrow (3,2,0)$. The shapes of the DCSs of these transitions, shown in Fig.5, are similar to the one in Fig.1a, and can be analysed in the same manner (see Supplementary Material C). We find that all three transitions share the same Regge trajectories, plotted in Fig.6. Such a coincidence is to be expected, as the singularities, whether in the CE or CAM plane, are shared by all matrix elements, which differ only in the magnitude of the corresponding residues. The $(0,0,0) \rightarrow (3,2,0)$ transition is, however, different in one respect. Its \tilde{f} - and \tilde{g} -amplitudes in Figs.9c,d reveal an additional minimum in the $0 \leq \varphi \leq \pi$ region across the whole energy range. This feature can be traced back to a *Regge zero* trajectory shown in Fig.10. The zero affecting the $(0,0,0) \rightarrow (3,2,0)$ transition is likely the cause of a somewhat poorer agreement with the rainbow theory in Fig.8c of Ref.[16]. A more detailed analysis of the $(0,0,0) \rightarrow (3,1,0)$ and $(0,0,0) \rightarrow (3,2,0)$ transitions will be given elsewhere [30].

In summary, the same resonance is responsible for the shape of the DCS in Fig.1a as well as in Figs.5a,b.

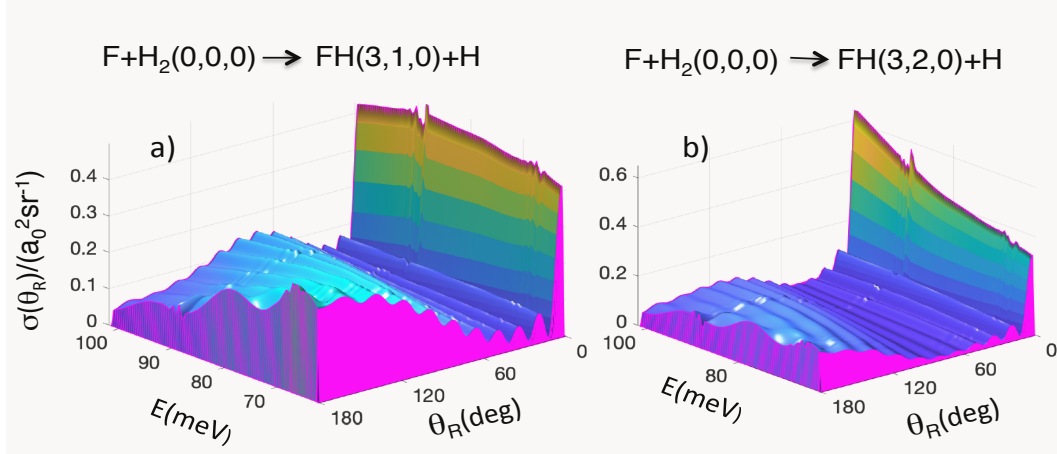


FIG. 5. a) Reactive differential cross section $\sigma_{\nu_f \leftarrow \nu_i}(\theta_R)$ for $\nu_i = (0, 0, 0)$ and $\nu_f = (3, 1, 0)$ vs. θ_R and E . b) Same as (a), but for $\nu_f = (3, 2, 0)$.

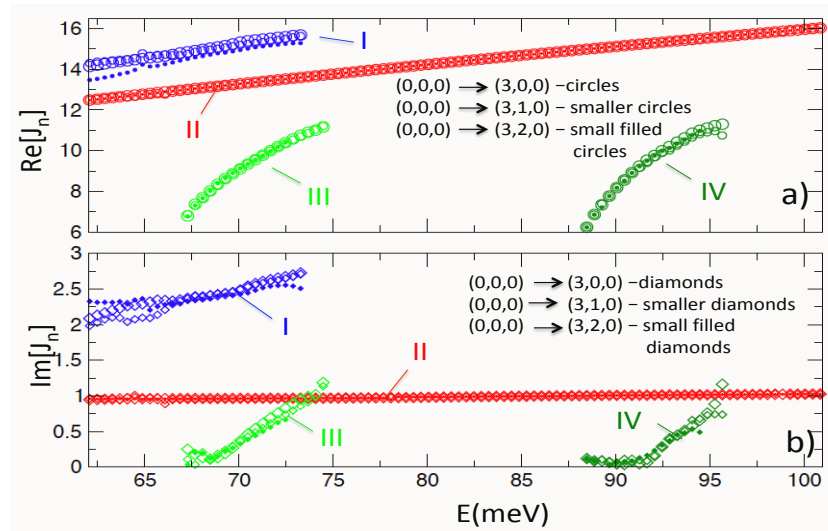


FIG. 6. a) Real parts of the Regge trajectories I, II, III, and IV (circles) for $\nu_i = (0, 0, 0)$ and $\nu_f = (3, 0, 0), (3, 1, 0), (3, 2, 0)$. b) Imaginary parts of the same trajectories (diamonds).

III. CONCLUSIONS AND DISCUSSION

A thorough analysis revealed that a single resonance is largely responsible for the unusual behaviour of the $F + H_2(0, 0, 0) \rightarrow FH(3, j, 0)$ reaction in the entire collision energy range 62.09 – 101.67 meV. This behaviour, we recall, involves a pronounced forward scattering maximum, followed by oscillations clearly visible at all scattering angles [cf. Figs.1 and 5]. The resonance has been identified as the transition state resonance A, extensively studied in

the Refs. [11]- [15],[9], to which we refer the interested reader. Its lifetime (i.e., the typical time the metastable complex exists prior to breaking up into products), $\tau = \hbar/2\text{Im}[E_I]$ is found to be rather short, $\approx 2 \times 10^{-16}$ sec. for $12 \leq J \leq 17$ [cf. Fig.6]. It is, however, premature to judge the resonance to be too short-lived to produce observable effects in the corresponding state-to state DCS. More important in this regard is its angular life $\phi = \hbar/2\text{Im}[J_I]$ (i.e., the angle by which the complex rotates before breaking up into products), otherwise given by the product of τ with the complex's angular velocity ω . The latter can be considerable for a light triatomic with a large rotational constant $B \approx \text{Re}[E_n]/J(J+1)$, and for the resonance A we find ϕ fairly stable, varying across the chosen energy range from 30.2° to 27.9° [cf. Fig.4]. However, even this relatively short angular life is proven to be sufficient to produce the interference patterns in the DCS [cf. Figs.1 and 5].

The resonance B, on the other hand, has a similar lifetime (cf. Fig.4), but a smaller rotational constant. Its rotation is slower, and the decay has little effect on sideways and backward scattering in Fig.3b and c. Still, we found it responsible for about 20% of the forward DCS in the 62 – 74 meV energy range, as shown in Fig.3a.

A similar behaviour is seen in the DCS of the three transitions considered here, $j_f = 0, 1, 2$. In all three cases, we found two other resonances, whose Regge trajectories were labelled III and IV. These, however, have only minor effect on the DCS, since their residues are too small, and the patterns they produced in the DCS are practically negligible.

Therefore, the three differential cross sections considered here give a fairly clear example of a single resonance, capable of dramatically changing the nature of reactive angular scattering. In the lower energy range $E < 62$ meV this conclusion is, however, no longer true, as both resonances A and B, are expected to play there equally important roles. We defer this case in our future work.

In conclusion, the proposed analysis, facilitated by the `DCS_Regge` code, can provide important insight into the reaction's mechanism. This paves the way for studying more complex chemical reactions.

IV. SUPPLEMENTARY MATERIAL

A. The unfolded amplitudes In the classical picture, Jacobi vector $\mathbf{R}_{A \leftarrow BC}$, drawn from the centre of mass of BC to A, rotates in the positive sense around the fixed direction of

the total angular momentum \mathbf{J} . For zero-helicity transition studied here, both the initial and final directions of $\mathbf{R}_{A\leftarrow BC}$, also lie in the plane. The winding angle φ , swept by the projection of $\mathbf{R}_{A\leftarrow BC}$ onto the plane, perpendicular to \mathbf{J} is simply related to the reactive scattering angle θ_R as shown in Fig.7a. For $0 < \varphi < \pi$ one has $\theta_R = \pi - \varphi$. However, the symmetry of the problem is such [20], that a rotation by $\varphi = \pi + \theta_R$ also leads to the same scattering angle. Adding multiples of 2π one obtains all winding angles in Eq.(5), consistent with the chosen θ_R . An angle $\varphi_m(\theta_R)$ falls into “nearside” or “farside” category, depending on whether m is even or odd, respectively.

In the body-fixed frame, used in the calculation of the S -matrix element, φ is the variable conjugate to J [28]. For this reason, transformations from J - to φ -representation in Eqs.(3) contain a simple exponential kernel $\exp(i\lambda\varphi)$. The full scattering amplitude is found by “folding back” the “unfolded amplitudes”, i.e., by summing with appropriate factors the values of $\tilde{f}(\varphi)$, or $\tilde{g}(\varphi)$, over all φ s consistent with the observational angle θ_R [cf. Eqs. (4)-(6)]. The procedure is illustrated schematically in Fig.7b.

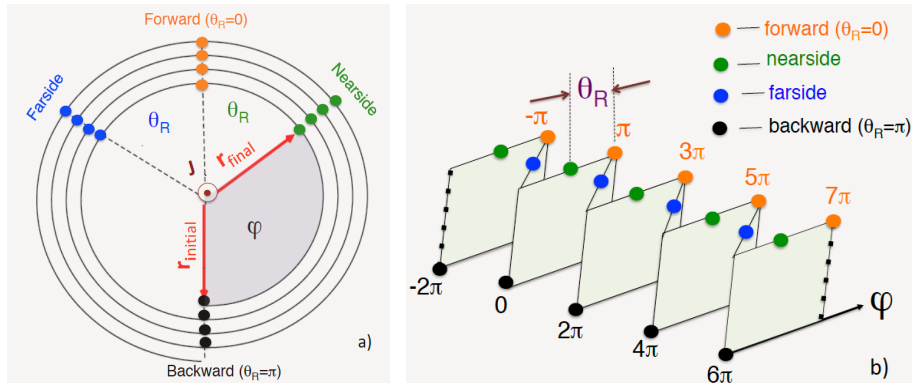


FIG. 7. a) Angle φ between the initial and final directions of a vector $\mathbf{r} = \mathbf{R}_{A\leftarrow BC}/|\mathbf{R}_{A\leftarrow BC}|$. Also shown other winding angles consistent with $0 < \theta_R < \pi$ (green and blue), $\theta_R = 0$ (orange), and $\theta_R = \pi$ (black). b) The values of φ_m over which $\tilde{f}(\varphi)$ is summed in Eq.(4) (green and blue), and the corresponding values for $\tilde{g}(\varphi)$ in Eqs.(6) (orange for $\theta_R = 0$, black for $\theta_R = \pi$).

B. Assignment of Regge resonances. Figure 8a shows the real parts of the complex energy poles of the resonances A and B, obtained by the Q-matrix analysis [14] for the Stark-Werner potential surface (triangles). Also shown by the filled circles are the CE poles obtained in the present work by the Padé reconstruction of $S_{3,0,0\leftarrow 0,0,0}^J$ for the FXZ PES. Both sets of poles agree if the spin-orbit correction of 12 meV (included in the FXZ, but not in the SW

PES), is subtracted from the SW results (see Fig.8b).

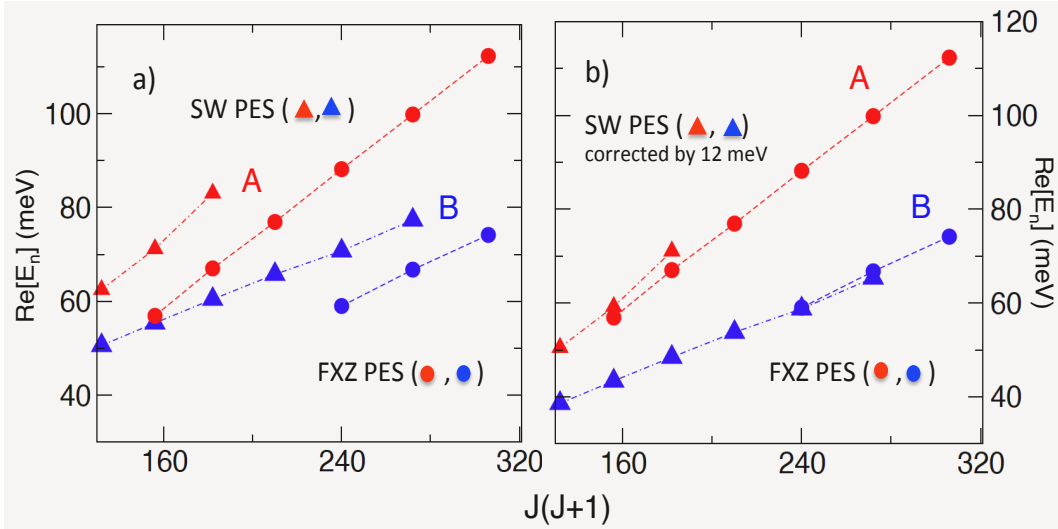


FIG. 8. a) The CE poles, obtained for Stark-Werner (SW) PES by the Q-matrix method of [14] (triangles) with the poles, obtained for the FXZ PES by the Padé reconstruction (circles, present work). The dashed lines show linear fits to the SW data. b) Same as (a), but with the SW poles shifted down by 12 meV.

C. Transitions $(0,0,0) \rightarrow (3,1,0)$ and $(0,0,0) \rightarrow (3,2,0)$. The amplitudes $\tilde{f}(\varphi, E)$ and $\tilde{g}(\varphi, E)$, shown in Fig.9, exhibit in the region $\varphi \geq \pi$ decaying tails, similar to those seen in Figs.1b and c. As in the case of the $(0,0,0) \rightarrow (3,0,0)$ we attribute them to the Regge trajectory II in Fig.6, corresponding to the resonance A of Sect.II B. The zeroes of $S_{3,2,0 \leftarrow 0,0,0}(J, E)$ in the complex J -plane are shown in Fig.10. One notes a regular zero trajectory, responsible for the trough in Figs.9c and d (highlighted). Also clearly visible are the zeroes which accompany Regge trajectories III and IV shown in Fig.6 (note that no zeroes accompany the pole trajectories I and II).

-
- [1] Kwei, G. H.; Herschbach, D. R. *J. Phys. Chem.* **1979**, *83*, 1550
[2] Neumark, D. M.; Wodtke, A. M.; Robinson, G. N.; Hayden, C. C.; Shobatake, K.; Sparks, R. K.; Schafer, T. P.; Lee, Y.T., *J.Chem.Phys.* **1985**, *85*, 3067
[3] Qiu, M.; Ren, Z.; Che, L., et al. *Science* **2006**, *311*, 1440
[4] Hu, W.; Schatz, G. C. *J. Chem. Phys.* **2006**, *125*, 132301

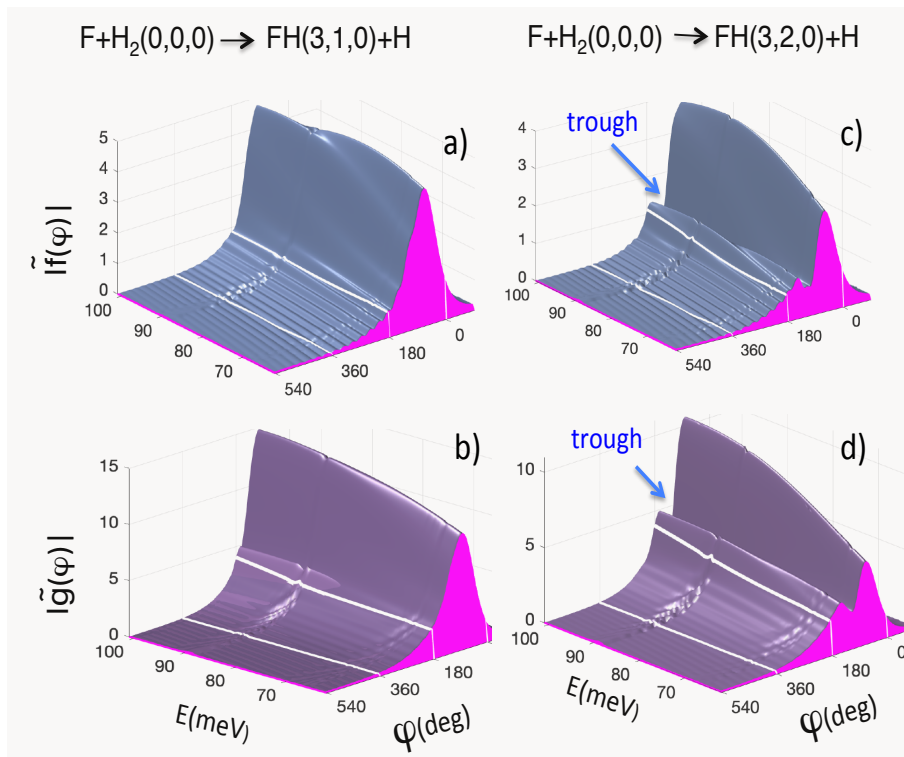


FIG. 9. a) The modulus of the unfolded amplitude $\tilde{f}(\varphi, E)$ for the $(0, 0, 0) \rightarrow (3, 1, 0)$ transition. b) The modulus of the unfolded amplitude $\tilde{g}(\varphi, E)$ for the $(0, 0, 0) \rightarrow (3, 1, 0)$ transition. c) Same as (a) but for the $(0, 0, 0) \rightarrow (3, 2, 0)$ transition. d) Same as (b) but for the $(0, 0, 0) \rightarrow (3, 2, 0)$ transition.

- [5] Rusin, L. Yu.; Sevryuk, M. B.; Toennies, J. P. *arXiv: 1009.1578v1* **2010**
- [6] Azriel', V. M.; Akimov, V. M.; Kolesnikova, L. I.; Rusin, L. Yu.; Sevryuk, M. B.; Toennies, J. P. *Khim. Fiz.* **2009**, *28*(11), 3. English translation: *Russ. J. Phys. Chem. B* **2009**, *3*, 857
- [7] Rusin, L. Yu.; Sevryuk, M. B.; Toennies, J. P. *Khim. Fiz.* **2007**, *26*(8), 11. English translation: *Russ. J. Phys. Chem. B* **2007**, *1*, 452
- [8] Rusin, L. Yu.; Sevryuk, M. B.; Toennies, J. P. *Khim. Fiz.* **2003**, *22*(9), 10
- [9] Castillo, J. F.; Manolopoulos, D. E.; Stark, K.; Werner, H.-J. *J. Chem. Phys.* **1996**, *104*, 6531
- [10] Manolopoulos, D. E. *J. Chem. Soc. Faraday Trans.* **1997**, *93*, 673
- [11] Chao, S. D.; Skodje, R. T. *J. Chem. Phys.* **2000**, *113*, 3487
- [12] Chao, S. D.; Skodje, R. T. *J. Chem. Phys.* **2003**, *119*, 1462
- [13] Aquilanti, V.; Cavalli, S.; De Fazio, D.; Volpi, A.; Aguilar, A.; Giménez, X.; Lucas, J. M., *Phys. Chem. Chem. Phys.* **2002**, *2*, 401

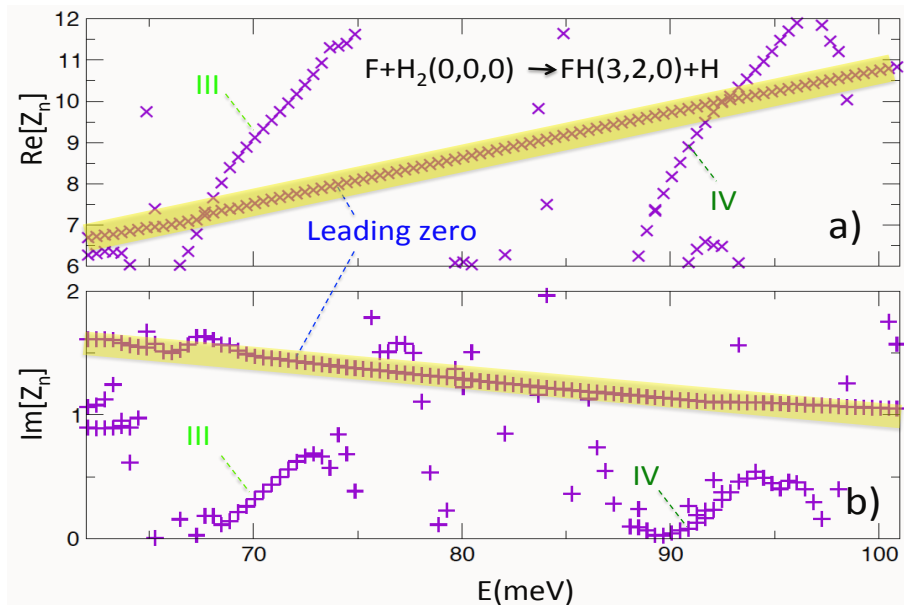


FIG. 10. a) Real parts of the CAM zeroes (crosses) of $S_{3,2,0 \leftarrow 0,0,0}$ vs. E . b) Same as (a) but for the zeroes' imaginary parts.

i

- [14] Aquilanti, V.; Cavalli, S.; Simoni, A.; Aguilar, A.; Lucas, J. M.; De Fazio, D. *J. Chem. Phys.* **2004**, *121*, 11675
- [15] Aquilanti, V.; Cavalli, S.; De Fazio, D.; Simoni, A.; Tscherbul, T. V. *J. Chem. Phys.* **2005**, *123*, 054314
- [16] Xiahou, Ch.; Connor, J. N. L.; De Fazio, D.; Sokolovski, D. *Phys. Chem. Chem. Phys.* **2024**, *26*, 3647
- [17] De Fazio, D., Cavalli, S., Aquilanti, V., Buchachenko, A. A., Tscherbul, T. V., *J. Phys. Chem. A*, **2007**, *111*, 12538
- [18] Skodje, R. T., D., Skouteris, D., Manolopoulos, D. E., Lee, S-H., Dong, F., Liu, J.T. *J. Chem. Phys. A*, **2000**, *112*, 4536
- [19] Skodje, R. T., D., Skouteris, D., Manolopoulos, D. E., Lee, S-H., Dong, F., Liu, J.T. *Phys. Rev. Lett. A*, **2000**, *85*, 1206
- [20] Akhmatskaya, E.; Sokolovski, D. *Comp. Phys. Comm.* **2022**, *277*, 108370
- [21] Brink, D. M. *Semiclassical Methods in Nucleus-Nucleus Scattering*, Cambridge University Press, Cambridge, **1985**
- [22] Sokolovski, D.; Akhmatskaya, E.; Sen, S. K. *Comp. Phys. Comm.* **2011**, *182*, 448

- [23] Sokolovski, D.; De Fazio, D.; Cavalli, S.; Aquilanti, V. *Phys. Chem. Chem. Phys.* **2007**, *9*, 5664
- [24] De Fazio, D. *Phys. Chem. Chem. Phys.* **2014**, *16*, 11662
- [25] Fu, B.; Xu, X.; Zhang, D. H. *J. Chem. Phys.* **2008**, *129*, 011103
- [26] Sokolovski, D.; Akhmatskaya, E.; Echeverría-Arrondo, C.; De Fazio, D. *Phys. Chem. Chem. Phys.* **2015**, *17*, 18577
- [27] Akhmatskaya, E.; Sokolovski, D.; Echeverría-Arrondo, C. *Comp. Phys. Comm.* **2014**, *185*, 2127
- [28] Sokolovski, D.; Connor, J. N. L. *Chem. Phys. Lett.* **1999**, *305*, 238
- [29] Sokolovski, D. *Phys. Rev. A.* **2000**, *62*, 024702
- [30] Xiahou, Ch.; Connor, J. N. L.; De Fazio, D., Akhmatskaya, E., and Sokolovski, D. (in preparation)

ACKNOWLEDGEMENTS

D.S. acknowledges financial support by the Grant PID2021-126273NB-I00 funded by MICINN/AEI/10.13039/501100011033 and by "ERDF A way of making Europe", as well as by the Basque Government Grant No. IT1470-22. D.DF acknowledges the CINECA award under the ISCRA initiative for the availability of high performance computing resources and support. E.A. acknowledges the financial support by MICIU/AEI/10.13039/501100011033 and FEDER, UE through BCAM Severo Ochoa accreditation CEX2021-001142-S / MICIU/ AEI / 10.13039/501100011033; PLAN COMPLEMENTARIO MATERIALES AVANZADOS 2022-2025, PROYECTO No:1101288, and grant PID2022-136585NB-C22; as well as by the Basque Government through ELKARTEK program under Grants KK-2023/00017, KK-2024/00062 and the BERC 2022-2025 program.